1

Catalytic Mechanism of C-F bond Cleavage: Insights from QM/MM Analysis of Fluoroacetate Dehalogenase

Yanwei Li[†], Ruiming Zhang[†], Likai Du[‡], Qingzhu Zhang[†*], Wenxing Wang[†]

[†]Environment Research Institute, Shandong University, Jinan 250100, P. R. China

[‡]Key Laboratory of Bio-based Materials, Qingdao Institute of Bio-energy and Bioprocess Technology, Chinese Academy of Sciences, Qingdao 266101, P. R. China

Keywords

_____

[*]Corresponding authors. E-mail: zqz@sdu.edu.cn

Fax: 86-531-8836 1990

1

Abstract

The catalytic mechanisms of fluoroacetate dehalogenase (FAcD) toward substrate fluoroacetate and chloroacetate were studied by combined quantum mechanics/molecular mechanics (QM/MM) method. There are twenty snapshots considered for each of the three individual systems. By analyzing multiple independent snapshots, positive or negative relationships between energy barriers and structural parameters in defluorination and dechlorination processes were established. We have also evidenced that conformational variations may cause enzymatic preference differences toward competitive pathways. Besides residues Arg111, Arg114, His155, Trp156, and Tyr219, the importance of residues His109, Asp134, Lys181, and His280 during the defluorination process were also highlighted through electrostatic analysis. These results may provide clues for designing new biomimetic catalysts toward degradation of fluorinated compounds.

1. Introduction

Fluorinated compounds are widely used in numerous industries and presently compose up to 20% of all pharmaceuticals and 30% of all the agochemicals (*1-3*). Its large-scale applications have caused increasingly environmental concerns due to its toxicity, global warming potential, environmental persistence, and bioaccumulation character (*4-6*). It is thus critically desiderated to set up strategies to minimize continued exposure of these fluorinated compounds. Environmental biotransformation, one of the most promising strategies with the lowest energy

44   consumption, has provided some encouraging results in cleaving the highly stable C-F

45   bond, whose dissociation energy is the highest among all the natural products (~130

46   kcal mol^{-1}) (*1*). For example, fluoroacetate dehalogenase (FAcD) discovered in

47   bacteria *Burkholdria sp.* FA1 was found to catalyze the dehalogenation process of its

48   natural substrate fluoroacetate (FAc) (*1*). FAc is very stable and toxic, and has been

49   widely manufactured and used as vertebrate pest control agents in many countries like

50   United States, Mexico, Australia, and New Zealand (*7-8*). Actually, the

51   dehalogenation process catalyzed by FAcD has embraced the most interests and

52   currently served as the model system for enzymatic defluorination investigations (*1,*

53   *9-18*).

54   The catalytic mechanism of FAcD has been investigated for many

55   decades, mainly by using site-directed mutagenesis and electrospray mass

56   spectrometry (*9-11*). Jitsumori et al. reported the first crystallization structure of FAcD

57   (from *Burkholdria sp.* FA1) which makes the mechanical elucidation of FAcD at the

58   molecular level possible (*13*). They also found that defluorination of FAcD requires a

59   catalytic triad Asp-His-Asp, and the aspartate acts as a nucleophile and directly ejects

60   the fluoride anion from FAc. Since the substrate FAc was not co-crystalized in the

61   crystal (PDB code 1Y37), Yashizawa and coworkers predicted the binding mode of

62   FAc with FAcD and investigated the subsequent mechanisms through Quantum

63   Mechanics/Molecular Mechanics (QM/MM) calculations (*14, 17*). In the two

64   excellent pioneer studies, the authors not only managed to determine the reaction

65   barrier of defluorination and dechlorination, but also explored the roles of residues

66   near the halide ion. However, the theoretically predicted binding mode of the substrate

67   is quite different from the binding mode found in the co-crystalized FAcD-FAc

68   complex (PDB code 3R3V) extracted in another bacterium *Rhodopseudomonas*

69   *palustris* CGA009 (*14, 16-17*). This inconformity raises interests to further investigate

70   the catalytic itinerary of FAcD (PDB code 3R3V) and answer the question that what

71   are the structural requirements that enables defluorination rather than dechlorination

72   (*16*). Understanding defluorination details of FAcD may be helpful in enzyme

73   engineering or biomimetic catalysis to remove harmful fluorinated compounds in the

74   environment. The relative locations of key active site residues and substrate FAc were

75   illustrated in Figure S1, ESI†.

76   Flexibility is one of the most intriguing characteristics of enzymes.

77   Recent room-temperature single molecule experiments have shown that enzyme

78   molecule exhibit large turnover rate fluctuations with a broad range of time scales (1

79   ms~100 s) (*19-20*). This leads to the proposal that each of the conformational states of

80   an enzyme is long-lived, and corresponds to a different turnover rate constant (*21-22*).

81   Thus, although it is still not common, considering multiple snapshots is highly

82   recommended when modelling enzymatic reactions (*23-25*). Multiple snapshots

83   should be considered when theoretically exploring why FAcD prefers defluorination

84   rather than dechlorination.

85   One of the main purposes of the current QM/MM analysis is to

86   investigate what are the structural requirements for FAcD (from bacterium

87   *Rhodopseudomonas palustris* CGA009, PDB code 3R3V) in enabling defluorination

88   rather than dechlorination by considering twenty snapshots. This may help in

89   designing *de novo* enzymes or biomimetic catalysts for degradation of other

90   fluorinated compounds. The present work also tries to provide solutions on how to

91   identify the two possible states of a neutrally charged histidine (Hsd155 or Hse155, as

92   shown in Scheme 1) of FAcD. This is valuable since currently there are still no better

93   solutions than visual inspection of the local hydrogen-bonding environment in

94   distinguishing these two neutrally charged states (*26*). In total, there are sixty reaction

95   pathways studied, forty for defluorination (with Hsd155 and Hsd155) and twenty for

96   dechlorination by FAcD.

2．Methods

2.1 MD Simulation

99   The initial models for the present simulation were built on the basis of

100   the X-ray crystal structure of $FAcD_{D110N}$-FAc binary complex (PDB code 3R3V,

101   resolution 1.50 Å) obtained from the Protein Data Bank (www.rcsb.org) (*16*). The

102   mutated residue (D110N) presented in the crystal structure was manually transformed

103   back into its natural form. The missing hydrogen atoms in the crystal structure were

104   added through CHARMM22 force field in the HBUILD module of CHARMM

105   package (*27-29*). The whole enzyme was dissolved in a water droplet (TIP3P model

106   (*30*)) with a radius of 35 Å. Then, the enzyme-water system was neutralized by

107   sodium ions via random substitution of solvent water molecules before being relaxed

108   through energy minimizations. The whole system was firstly heated from absolute

109   zero to 298.15 K in 50 ps (1 fs/step) and equilibrated thermally for 500 ps (1 fs/step)

110   to reach the equilibration state. After that, a 10 ns stochastic boundary molecular

111   dynamics (SBMD) simulation was performed at 298.15 K by using NVT ensemble for

112   conformational sampling (*31*). During the SBMD simulations, the whole system

113   moves freely except the substrate, the coordinates of which are restrained to keep

114   consistence with its positions in the crystal structure. The leap-frog algorithm and

115   Langevin temperature coupling method implemented in CHARMM program were

116   applied during the simulations. The obtained root-mean-square deviation was

117   provided in Figure S2, ESI†.

118   **2.2 QM/MM Calculations**

119   The QM/MM calculations were performed by using ChemShell (*32*)

120   platform, which can integrate programs Turbomole (*33*) and DL-POLY (*34*). The

121   charge shift model (*35*) and electrostatic embedding method (*36*) were used during the

122   QM/MM calculations. The geometries of the intermediates were optimized by using

123   hybrid delocalized internal coordinates optimizer while transition state searches were

124   done   by   using   microiterative   TS   optimizer   under   the

125   B3LYP/6-31G(d,p)//CHARMM22 level (*37*). Frequency calculations were performed

126   to validate the one imaginary frequency character of transition state structures, and the

127   suitability of the transition vector was also confirmed. Additional single point energy

128   calculations were carried out at the RIMP2/cc-pVTZ//CHARMM22 level for better

129   description of the energy profiles.

130   Three systems have been investigated in the present study. For

131   convenience of the description, they are named as FAcD$_{Hsd155}$-FAc, FAcD$_{Hse155}$-FAc,

132   and FAcD$_{Hse155}$-ClAc. The QM regions contain residues Asp110, Arg111, His155,

133   Trp156, Tyr219, a water molecule, and substrate (FAc or ClAc), as labeled in Scheme

134   1. This resulted in 90 QM atoms in total. For all these three systems, the MM atoms

135   within 20 Å of element F or Cl were allowed to move while the other MM atoms were

136   fixed during the QM/MM calculations. Twenty snapshots extracted from the 10 ns

137   molecular dynamics trajectory with an interval of 0.5 ns for each of the three systems.

138   **2.3 Boltzmann-weighted Average**

139   To analyze the computed energy barrier spreads among twenty

140   snapshots, the average barrier were calculated by Boltzmann-weighted average

141   method (*38-40*):

142
$$\Delta E = -RT \ln \left\{ \frac{1}{n} \sum_{i=1}^{n} \exp\left(\frac{-\Delta E_i}{RT} \right) \right\}$$

143   Where, ΔE is the average barrier, R is gas constant, n is the number of

144   snapshots, ΔE_i is the energy barrier of path i, and T is the temperature. For a small n,

145   if the set of starting geometries happens to include one with an anomalously low

146   energy barrier, this will have a disproportionate effect on the Boltzmann-weighted

147   average barrier. The disproportionate effect can be evaluated by the following

148   equation:

149
$$DE = \frac{\Delta E^{a-l} - \Delta E^{a}}{\Delta E^{a}} \times 100\%$$

150   Where *DE* represents for the disproportionate effect, ΔE^{a-l} is the

151   Boltzmann-weighted average barrier calculated by neglecting the snapshot with the

152   lowest energy barrier, ΔE^{a} is the Boltzmann-weighted average barrier with all the

153   snapshots considered.

154   **3．Results and Discussion**

155   The first step of this work is to identify the reliability of the calculation

156   method. Due to the absence of the X-ray crystal structure of the $FAcD_{wild}$-FAc binary

157   complex, it is difficult to make a direct comparison between the calculated results and

158   the experimental data. To verify the reliability of the computational results, we

159   optimized the available crystal structure of $FAcD_{D110N}$-FAc binary complex at the

160   B3LYP/6-31G(d,p)//CHARMM22 level. The calculated results agree well with the

161   available experimental values. For example, the spatial distances of N_{α}-O_{β}, O_{β}-C_{γ},

162   C_{γ}-C_{δ}, and C_{δ}-F are 2.79, 1.26, 1.52, and 1.44 Å, in accordance with the X-ray data of

163   2.98, 1.19, 1.54, and 1.42 Å (Atomistic labels are shown in Scheme 1) (*16*).

164   Consequently, it might be inferred that the choice of the B3LYP/6-31G(d,p) method

165   for QM region geometric optimizations is appropriate in the present study.

166   **3.1 Reaction Mechanism and Potential Energy Profiles**

167   The one-step dehalogenation reaction of FAcD toward FAc was shown

168   in Scheme 1. The reaction is triggered by a negatively charged residue Asp110.

169   Asp110 acts as a nucleophile and attacks C_{δ} atom of substrate FAc, which eventually

170   lead to the C-F bond cleavage and F ion elimination, similar with the previously

171   proposed dehalogenation mechanism (*14*). However, the binding mode of substrate

172   FAc is different, as indicated in Figure S1 (a~d) and Table S1, ESI†. In addition, a

173   water molecule was found to stabilize the leaving F ion through a hydrogen bond,

174   which has not been reported (*14*). It is likely that this water molecule is crucial in the

175   ejection process of the F ion, as indicated in Figure S1 (e), ESI†. More structural

176   analysis on the dehalogenation itineraries will be discussed in the following section.

177   For system $FAcD_{Hsd155}$-FAc, a substantial energy barrier spread, 12.5~26.8 kcal mol^{-1},

178   among twenty different snapshots has been found. Similar substantial energy barrier

179   spreads for systems $FAcD_{Hse155}$-FAc (9.7~21.5 kcal mol^{-1}) and $FAcD_{Hse155}$-ClAc

180   (13.0~23.6 kcal mol^{-1}) were also found. By assuming that each snapshot extracted

181   from the dynamics trajectory corresponds to a local rate constant (*41*), these

182   calculated energy barrier fluctuations may be helpful in rationalizing recent single

183   molecule experiment findings that the reaction rate of a single enzyme molecule is not

184   constant but exhibits large fluctuations with a broad range (*19-20, 22, 39*).

185   The Boltzmann-weighted average barriers, energy barrier spreads, and

186   the disproportionate effects for the three systems were provided in Table 1. The

187   detailed barriers and imaginary frequencies for each reaction pathway were provided

188   in Table 2. No anomalously low energy barriers were found for all the three systems,

189   as indicated by the low value of disproportionate effects (2.9%, 8.8%, and 4.8%). The

190   Boltzmann-weighted average barrier of system $FAcD_{Hsd155}$-FAc is 13.8 kcal mol^{-1},

191   which is 2.4 kcal/mol higher than that of system $FAcD_{Hse155}$-FAc. This implies that

192    $FAcD_{Hse155}$ structure is slightly feasible than $FAcD_{Hsd155}$. By analyzing the energy

193   barriers of twenty different snapshots, about 70% of the barriers in system

194   FAcD$_{Hsd155}$-FAc were found to be higher than the barriers in corresponding snapshots

195   in system FAcD$_{Hse155}$-FAc, as shown in Table 2. Although it is credible at a relatively

196   high ratio (about 70%) in predicting the feasibility of competitive pathways by using a

197   single snapshot, errors may also occur. For example, if only snapshot 6 ns is used in

198   distinguishing the competitive pathways, error occurs: FAcD$_{Hsd155}$ (ΔE=14.6 kcal

199   mol^{-1}) may seem more feasible than FAcD$_{Hse155}$ (ΔE=19.3 kcal mol^{-1}).

200   The following dehalogenation investigations toward substrate FAc and

201   ClAc were mainly investigated on the basis of structure FAcD$_{Hse155}$ since it is

202   energetically feasible than structure FAcD$_{Hsd155}$. The Boltzmann-weighted average

203   barrier of system FAcD$_{Hse155}$-FAc (11.4 kcal mol^{-1}) is 3.1 kcal/mol lower than that of

204   system FAcD$_{Hse155}$-ClAc (14.5 kcal mol^{-1}), which indicates that defluorination is more

205   feasible than dechlorination. Interestingly, gas phase calculations (without protein

206   environment) performed at the RIMP2/cc-pVTZ//B3LYP/6-31G(d,p) level by using

207   Gaussian 09 program (*42*) showed that energy barriers for defluorination (105.8 kcal

208   mol^{-1}) is 33.1 kcal/mol higher than that of dechlorination (72.7 kcal/mol) (Scheme S1,

209   ESI†). By considering the contribution from side chains of Arg111 and Arg114,

210   significant lower barriers were found for defluorination (37.7 kcal mol^{-1}) and

211   dechlorination (18.1 kcal mol^{-1}). This highlights the importance of residues Arg111

212   and Arg114 in dehalogenation reactions. However, residues Arg111 and Arg114 are

213   not responsible for the fact that FAcD prefers defluorination (11.4 kcal mol^{-1}) rather

214   than dechlorination (14.5 kcal mol^{-1}). Discussions on this issue will be provided in

215 detail in the following paragraphs through both structural and energetic aspects.

3.2 Dehalogenation Itineraries

217 Among all the twenty studied snapshots, six snapshots with lowest

218 energy barriers in systems $FAcD_{Hse155}$-FAc (0.5 ns, 1.5 ns, 2.5 ns, 4 ns, 6.5 ns, and 7.5

219 ns) and $FAcD_{Hse155}$-ClAc (0.5 ns, 4 ns, 4.5 ns, 6 ns, 7 ns, and 9.5 ns) were chosen for

220 the following dehalogenation itinerary investigations. The variations of two crucial

221 geometry parameters, angle $O_{\varepsilon}C_{\delta}X$ and dihedral $O_{\omega}C_{\gamma}C_{\delta}O_{\varepsilon}$, along the dehalogenation

222 processes (indicated by bond C_{δ}-X increase) were provided in Figure 1. For a more

223 direct view, the spatial locations of active site residues in the structures of reactants,

224 transition states and products for systems $FAcD_{Hse155}$-FAc (4 ns, ΔE=9.7 kcal mol^{-1})

225 and $FAcD_{Hse155}$-ClAc (4.5 ns, ΔE=13.0 kcal mol^{-1}) were representatively displayed in

226 Figure 2 and Figure S3, respectively. Figure 2 shows that residues Arg111 and Arg114

227 provide hydrogen network stabilization for the carboxy group of FAc or ClAc while

228 residues His155, Trp156, and Tyr219 provide stabilization for F or Cl. As shown in

229 Figure 1, the calculated C_{δ}-X bond distances in the reactant structures of systems

230 $FAcD_{Hse155}$-FAc (1.42~1.44 Å) and $FAcD_{Hse155}$-ClAc (1.84~1.85 Å), and the

231 calculated dihedral $O_{\omega}C_{\gamma}C_{\delta}O_{\varepsilon}$ in the products of system $FAcD_{Hse155}$-FAc

232 (162.7~175.4°) are all in promising agreement with the available crystal data (1.42 Å,

233 1.79 Å, and 172.2°, respectively) (*16*). The angles of $O_{\varepsilon}C_{\delta}F$ and $O_{\varepsilon}C_{\delta}Cl$ in the

234 transition states locate at the range of 161.0~166.8° and 149.3~157.9°, which are

235 slightly deviated from the theoretical value (180°) for an S_N2 reaction. Another

236 interesting issue is the variation of dihedral $O_\omega C_\gamma C_\delta O_\varepsilon$. Previous *ab initio* calculations

237 in free solutions indicate an orthogonal direction (~90°) of the dihedral $O_\omega C_\gamma C_\delta O_\varepsilon$

238 during the dehalogenation process, while the crystal data of the product (3R3Y,

239 resolution 1.15 Å) indicate a nearly coplanar dihedral $O_\omega C_\gamma C_\delta O_\varepsilon$ (172.2°) (*43*).

240   To get a more comprehensive understanding, more analysis on the

241 dehalogenation process were performed, and a dynamic property of dihedral

242 $O_\omega C_\gamma C_\delta O_\varepsilon$ during the dehalogenation processes was found. For example, $O_\omega C_\gamma C_\delta O_\varepsilon$

243 varies from 112.6~124.4° (reactants) to 125.1~138.6° (transition states) and finally to

244 162.7~175.4° (products) during defluorination processes by enzyme FAcD. In

245 addition, the natural population analysis (NPA) on systems $FAcD_{Hse155}$-FAc and

246 $FAcD_{Hse155}$-ClAc were performed and the natural charge variations are provided in

247 Table S2, ESI†. The natural charges of the halide atoms in two systems are

248 significantly different: natural charges of atom F changes from -0.43±0.02 to

249 -0.73±0.04 while the natural charges of atom Cl changes from -0.18±0.02 to

250 -0.89±0.02 during the dehalogenation processes. The natural charges of halide ions in

251 the products indicate a better stabilization of FAcD toward F (-0.73±0.04) than Cl

252 (-0.89±0.02).

253 **3.3 Potential Energy Profiles versus Key Structural Parameters**

254   To gain a more comprehensive understanding between potential energy

255 profiles and structural parameters, twenty energy barriers in both defluorination and

256 dechlorination reactions as a function of the corresponding angle $O_\varepsilon C_\delta X$ (X=F or Cl)

257   variations (from reactants to transition states), the values of angle $O_\varepsilon C_\delta X$ in the

258   reactants, and the values of angle $O_\varepsilon C_\delta X$ in the transition states were provided, as

259   shown in Figure 3. Although it is not possible to establish a precise correlation, in

260   some way the barriers tend to increase as the angle $O_\varepsilon C_\delta X$ variations becomes larger

261   (Fig. 3a). Since distribution ranges of angle $O_\varepsilon C_\delta X$ in the transition states (within 10°)

262   are about two or three times narrower than that in the   reactants, the established

263   barrier increasing tendency was mainly associated with the value of angle $O_\varepsilon C_\delta X$ in

264   reactants, as shown in Figure 3b and 3c. This may at least provide one suggestion for

265   biomimetic catalyst or *de novo* enzyme designing in enhancing the C-F or C-Cl bond

266   cleavage: try to increase the value of angle $O_\varepsilon C_\delta X$ in the reactant structures. The

267   relatively   smaller   angles   of $O_\varepsilon C_\delta Cl$ (91.2~118.3°)   compared   with $O_\varepsilon C_\delta F$

268   (119.5~132.5°) in the reactants were mainly due to the improper binding of ClAc in

269   the smaller active site pocket designed for accommodating the natural substrate (FAc)

270   of FAcD. This highlights the importance of residues Arg111, Arg114, His155, Trp156,

271   and Tyr219 during the dehalogenation processes. For example, mutations of

272   Arg111Lys or His155Asn may change the topology of the active site and increase the

273   angle values. Plots displaying the potential energy barriers versus different structural

274   parameters (such as dihedral $O_\omega C_\gamma C_\delta O_\varepsilon$ and bond $O_\varepsilon C_\delta$) were provided in Figures S4

275   and S5 for searching any other promising correlation between barrier and structure.

276   **3.4 Residue Electrostatic Influence**

277   The activation energy difference caused by amino acid i can be

278   described as:

279   $$\Delta E^{i-0} = \Delta E^i - \Delta E^0$$

280   Where ΔE^{i-0} is the changes of the barrier, ΔE^i is the energy barrier with

281   charges on residue i set to 0, and ΔE^0 is the original values of the energy barrier. For

282   analyzing a QM region residue, the residue should be firstly excluded from the QM

283   region. During all these calculations, the geometry structures of the stationary points

284   were kept unchanged. A positive ΔE^{i-0} value means that neglecting the influence of the

285   i^{th} residue will increase the energy barrier. In other words, a positive ΔE^{i-0} value means

286   the ith residue lowers the energy barrier and facilities the catalytic reaction.

287   The electrostatic influences of twenty residues on defluorination and

288   dechlorination processes were schematically represented in Figure 4. The electrostatic

289   contacts from residues His155, Trp156, and Tyr219 have been proposed to be

290   important in dehalogenation processes of FAcD (*14*), which was confirmed in the

291   present study. Additionally, the electrostatic influences of His155, Trp156, and Ty219

292   on defluorination are much stronger than on dechlorination. Our analysis also

293   highlights four residues (His109, Asp134, Lys181, and His280) for defluorination

294   reactions and two residues (His109 and His280) for dechlorination reactions. These

295   residues have a strong electrostatic influence to the reaction barrier (-2.0 kcal mol^{-1} <

296   ΔE^{i-0} < 2.0 kcal mol^{-1}) and may serve as candidate residues for the following mutation

297   studies. The other residues were found with relatively weaker electrostatic influence

298   to the reaction barrier.

299   **4. Conclusions**

14

300   By analyzing the energy barriers of twenty snapshots and comparing the

301   Bolzmann weighted average barriers, we proved that structure $FAcD_{Hse155}$ is more

302   energetically feasible than structure $FAcD_{Hsd155}$ for enzyme FAcD while $FAcD_{Hse155}$

303   prefers defluorination rather than dechlorination process. A positive correlation

304   between energy barriers and key structural parameter (angle $O_\varepsilon C_\delta X$) was found. This

305   may help biomimetic catalyst or *de novo* enzyme designing in enhancing the C-F or

306   C-Cl bond cleavage. Besides residues Arg111, Arg114, His155, Trp156, and Tyr219,

307   the important role of residues His109, Asp134, Lys181, and His280 during the

308   defluorination process were also highlighted. In addition, we found that

309   conformational variations may cause different enzymatic preferences toward

310   competitive pathways. Thus, studying only one snapshot in distinguishing competitive

311   reaction pathways is not reliable.

References

313   1 P. Goldman, *Science*, 1969, **164**, 1123-1130.

314   2 K. Muller, C. Faeh and F. Diederich, *Science*, 2007, **317**, 1881–1886.

315   3 B. D. Key, R. D. Howell, and C. S. Criddle, *Environ. Sci. Technol.*, 1997, **31**,

316   2445–2454.

317   4 C. Douvris and O. V. Ozerov, *Science*, 2008, **321**, 1188–1190.

318   5 A. M. Calafat, L. Y. Wong, Z. Kuklenyik, J. A. Reidy, and L. L. Needham, *Environ.*

319   *Health. Perspect.*, 2007, **115**, 1596–1602.

320   6 M. Houde, J. W. Martin, R. J. Letcher, K. R. Solomon, and D. C. Muir, *Environ. Sci.*

321   *Technol.*, 2006, **40**, 3463–3473.

322   7 X. Zhang, T. Lai, and Y. Kong, *Top. Curr. Chem.*, 2012, **308**, 365–404.

323   8 A. T. Proudfoot, S. M. Bradberry, and J. A. Vale, *Toxicol. Rev.*, 2006, **25**, 213–219.

324   9 J. Q. Liu, T. Kurihara, S. Ichiyama, M. Miyagi, S. Tsunasawa, H. Kawasaki, K.

325   Soda, and N. Esaki, *J. Biol. Chem.*, 1998, **273**, 30897–30902.

326   10 T. Kurihara and N. Esaki, *Chem. Rec.*, 2008, **8**, 67–74.

327   11 T. Kurihara, T. Yamauchi, S. Ichiyama, H. Takahata, and N. Esaki, *J. Mol. Catal. B:*

328   *Enzymatic*, 2003, **23**, 347–355.

329   12 Y. Zhang, Z. S. Li, J. Y. Wu, M. Sun, Q. C. Zheng, and C. C. Sun, *Biochem.*

330   *Biophys. Res. Commun.*, 2004, **325**, 414–420.

331   13 K. Jitsumori, R. Omi, T. Kurihara, A. Kurata, H. Mihara, I. Miyahara, K. Hirotsu,

332   and N. Esaki, *J. Bacteriol.*, 2009, **191**, 2630–2637.

333   14 T. Kamachi, T. Nakayama, O. Shitamichi, K. Jitsumori, T. Kurihara, N. Esaki, and

334   K. Yoshizawa, *Chem. Eur. J.*, 2009, **15**, 7394–7403.

335   15 P. W. Y. Chan, M. Wong, J. Guthrie, A. V. Savchenko, A. F. Yakunin, E. F. Pai, and

336   E. A. Edwards, *Microb. Biotechnol.* 2010, **3**, 107–120

337   16 P. W. Y. Chan, A. F. Yakunin, E. A. Edwards, and E. F. Pai, *J. Am. Chem. Soc.* 2011,

338   **133**, 7461–7468.

339   17 T. Nakayama, T. Kamachi, K. Jitsumori, R. Omi, K. Hirotsu, N. Esaki, T. Kurihara,

340   and K. Yoshizawa, *Chem. Eur. J.*, 2012, **18**, 8392–8402.

341   18 C. K. Davis, R. I. Webb, L. I. Sly, S. E. Denman, and C. S. McSweeney, *FEMS*

342   *Microbiol. Ecol.*, 2012, **80**, 671–684.

343   19 H. P. Lu, L. Xun, and X. S. Xie, *Science*, 1998, **282**, 1877–1882.

344   20 W. Min, B. P. English, G. Luo, B. J. Cherayil, S. C. Kou, and X. S. Xie, *Acc. Chem.*

345   *Res.*, 2005, **38**, 923–931.

346   21 H. Yang, G. Luo, P. Karnchanaphanurach, T. M. Louie, I. Rech, S. Cova, L. Xun,

347   and X. S. Xie, *Science*, 2003, **302**, 262–266.

348   22 X. S. Xie, *Science*, 2013, **342**, 1457–1459.

349   23 A. Warshel, P. K. Sharma, M. Kato, Y. Xiang, H. Liu, and M. H. Olsson, *Chem.*

350   *Rev.* 2006, **106**, 3210–3235.

351   24 H. M. Senn and W. Thiel, *Angew. Chem. Int. Ed.*, **2009**, 48, 1198–1229.

352   25 G. G. Hammes, S. J. Benkovic, and S. Hammes-Schiffer, *Biochemistry*, 2011, **50**,

353   10422–10430.

354   26 R. Lonsdale, J. N. Harvey, and A. J. Mulholland, *Chem. Soc. Rev.* 2012, **41**,

355   3025–3038.

356   27 B. R. Brooks, R. E. Bruccoleri, B. D. Olafson, D. J. States, S. Swaminathan, and M.

357   Karplus, *J. Comput. Chem.*, 1983, **4**, 187–217.

358   28 B. R. Brooks, C. L. Brooks III, A.D. Mackerell, L. Nilsson, R. J. Petrella, B. Roux,

359   Y. Won, G. Archontis, C. Bartels, S. Boresch, A. Caflisch, L. Caves, Q. Cui, A. R.

360   Dinner, M. Feig, S. Fischer, J. Gao, M. Hodoscek, W. Im, K. Kuczera, T. Lazaridis,

361   J. Ma, V. Ovchinnikov, E. Paci, R. W. Pastor, C. B. Post, J. Z. Pu, M. Schaefer, B.

362   Tidor, R. M. Venable, H. L. Woodcock, X. Wu, W. Yang, D. M. York, and M.

363   Karplus, *J. Comp. Chem.*, 2009, **30**, 1545–1615.

364   29 A. D. MacKerell, B. Brooks, C. L. Brooks, L. Nilsson, B. Roux, Y. Won, and M.

365   Karplus, John Wiley & Sons, New York, **1998**.

366   30 W. L. Jorgensen, J. Chandrasekhar, J. D. Madura, R. W. Impey, and M. L. Klein, *J.*

367   *Chem. Phys.*, 1983, **79**, 926–935.

368   31 C. L. Brooks, and M. Karplus, *J. Chem. Phys.*, 1983, **79**, 6312–6325.

369   32 P. Sherwood, A. H. D. Vries, M. F. Guest, G. Schreckenbach, C. R. A. Catlow, S. A.

370   French, A. A. Sokol, S. T. Bromley, W. Thiel, A. J. Turner, S. Billeter, F. Terstegen,

371   S. Thiel, J. Kendrick, S. C. Rogers, J. Casci, M. Watson, F. King, E. Karlsen, M.

372   Sjovoll, A. Fahmi, A. Schafer, and C. Lennartz, *J. Mol. Struc-Theochem.*, 2003,

373   **632**, 1–28.

374   33 R. Ahlrichs, M. Bär, M. Häser, H. Horn, and C. Kölmel, *Chem. Phys. Lett.*, 1989,

375   **162**, 165–169.

376   34 W. Smith and T. R. Forester, *J. Mol. Graphics.*, 1996, **14**, 136–141.

377   35 A. H. de Vries, P. Sherwood, S. J. Collins, A. M. Rigby, M. Rigutto, and G. J.

378   Kramer, *J. Phys. Chem. B*, 1999, **103**, 6133–6141.

379   36 D. Bakowies and W. J. Thiel, *Phys. Chem.*, 1996, **100**, 10580–10594.

380   37 S. R. Billeter, A. J. Turner, and W. Thiel, *Phys. Chem. Chem. Phys.*, 2000, **2**,

381   2177–2186.

382   38 R. Lonsdale, J. N. Harvey, A. and J. Mulholland, *J. Phys. Chem. B*, 2010, **114**,

383   1156–1162.

384   39 Y. Li, X. Shi, Q. Zhang, J. Hu, J. Chen, and W. Wang, *Environ. Sci. Technol.*, 2014,

385   **48**, 5008–5016.

386   40 Y. Li, R. Zhang, L. Du, Q. Zhang, W. Wang, *RSC adv.*, **2015**, 5, 13871–13877.

387   41 P. Saura, R. Suardíaz, L. Masgrau, J. M. Lluch, and À. González-Lafont, *ACS*

388   *Catal.*, 2014, **4**, 4351–4363.

389   42 M. J. Frisch, G. W. Trucks, H. B. Schlegel, G. E. Scuseria, M. A. Robb, J. R.

390   Cheeseman, G. Scalmani, V. Barone, B. Mennucci, G. A. Petersson, H. Nakatsuji,

391   M. Caricato, X. Li, H. P. Hratchian,;A. F. Izmaylov,. Bloino, G. Zheng, J. L.

392   Sonnenberg, M. Hada, M. Ehara, K. Toyota, R. Fukuda, J. Hasegawa, M. Ishida, T.

393   Nakajima, Y. Honda, O. Kitao, H. Nakai, T. Vreven, J. A. Jr. Montgomery, J. E.

394   Peralta, F. Ogliaro, M. Bearpark, J. J. Heyd, E. Brothers, K. N. Kudin, V. N.

395   Staroverov, R. Kobayashi, J. Normand, K. Raghavachari, A. Rendell, J. C. Burant,

396   S. S. Iyengar, J. Tomasi, M. Cossi, N. Rega, J. M. Millam, M. Klene, J. E. Knox, J.

397   B. Cross, V. Bakken, C. Adamo, J. Jaramillo, R. Gomperts, R. E. Stratmann, O.

398   Yazyev, A. J. Austin, R. Cammi, C. Pomelli, J. W. Ochterski, R. L. Martin, K.

399   Morokuma, V. G. Zakrzewski, G. A. Voth, P. Salvador, J. J. Dannenberg, S.

400   Dapprich, A. D. Daniels, O. Farkas, J. B. Foresman, J. V. Ortiz, J. Cioslowski, and

401   D. J. Fox, Gaussian 09, revision A.02; Gaussian, Inc.: Wallingford, CT, **2009**.

402   43 R. D. Bach, B. A. Coddens, and G. J. Wolber, *J. Org. Chem.*, 1986, **51**, 1030–1033.

403

404

405

406

407

408

Acknowledgements

Electronic Supplementary Information

Hydrogen bond distances between FAcD and the substrates (Table S1), NPA charge variations (Table S2), gas phase calculations (Scheme S1); binding of FAc with FAcD (Figure S1), root-mean-square deviation (Figure S2), structures involved in dechlorination process of system $FAcD_{Hse155}$-ClAc (Figure S3), correlation between potential energy barriers and dihedral $O_{\omega}C_{\gamma}C_{\delta}O_{\varepsilon}$ (Figure S4), and correlation between potential energy barriers and bond $O_{\varepsilon}C_{\delta}$ (Figure S5).

430   **Table 1** Energy barrier spreads, Boltzmann weighted average barriers, and

431   disproportionate effects calculated at RIMP2/cc-pVTZ//CHARMM22 level for the six

432   studied systems

433

Systems	Barrier spreads/(kcal/mol)	Boltzmann-weighted average barriers/(kcal mol^{-1})	Disproportionate effects
FAcD$_{Hsd155}$-FAc	12.5~26.8	13.8	2.9%
FAcD$_{Hse155}$-FAc	9.7~21.5	11.4	8.8%
FAcD$_{Hse155}$-ClAc	13.0~23.6	14.5	4.8%

434
435
436
437
438
439
440
441
442
443
444
445
446
447
448
449
450
451
452
453
454
455
456
457
458
459
460
461
462
463
464
465
466
467

468   **Table 2** Energy barriers and imaginary frequencies for twenty snapshots of systems

469   FAcD$_{Hsd155}$-FAc,   FAcD$_{Hse155}$-FAc,   and   FAcD$_{Hse155}$-FAc   calculated   at

470   RIMP2/cc-pVTZ//CHARMM22 level

471

Systems	FAcD$_{Hsd155}$-FAc		FAcD$_{Hse155}$-FAc		FAcD$_{Hse155}$-ClAc	
Snapshots/ns	Barrier/ (kcal mol^{-1})	Imaginary frequency/ (cm^{-1})	Barrier/ (kcal mol^{-1})	Imaginary frequenc/ (cm^{-1})	Barrier/ (kcal mol^{-1})	Imaginary frequenc/ (cm^{-1})
0.5	12.5	315i	14.3	294i	15.4	213i
1	18.9	312i	18.6	327i	17.8	239i
1.5	19.6	317i	15.1	298i	20.4	211i
2	22.6	329i	20.2	302i	17.6	251i
2.5	19.1	307i	10.7	330i	19.2	226i
3	21.7	297i	20.5	281i	17.4	215i
3.5	21.4	311i	16.0	309i	19.8	209i
4	20.7	321i	9.7	277i	13.6	199i
4.5	19.8	299i	15.5	289i	13.0	224i
5	22.1	329i	17.8	297i	18.5	231i
5.5	26.8	311i	21.9	301i	23.3	224i
6	14.6	300i	19.3	276i	14.8	218i
6.5	12.7	285i	15.0	296i	23.6	212i
7	22.6	333i	16.5	306i	14.6	217i
7.5	27.9	311i	15.3	292i	23.4	282i
8	13.1	352i	16.9	314i	18.0	176i
8.5	16.2	305i	16.5	309i	19.4	274i
9	18.4	308i	16.2	295i	21.0	247i
9.5	25.3	331i	21.5	308i	17.2	243i
10	25.4	328i	20.3	286i	20.0	252i

472
473
474
475
476
477
478
479
480
481
482
483
484

Figure Captions

Scheme 1 The QM regions in the reactants of three studied systems (FAcD$_{Hsd155}$-FAc, FAcD$_{Hse155}$-FAc, and FAcD$_{Hse155}$-FAc) and the dehalogenation processes of system FAcD$_{Hse155}$-FAc. The boundary between the QM and MM regions are indicated by wavy lines.

Figure 1 Variations of angles O$_\varepsilon$C$_\delta$F and O$_\varepsilon$C$_\delta$Cl, dihedrals O$_\omega$C$_\gamma$C$_\delta$O$_\omega$ for six snapshots with the lowest energy barriers in systems FAcD$_{Hse155}$-FAc (0.5 ns, 1.5 ns, 2.5 ns, 4 ns, 6.5 ns, and 7.5 ns) and FAcD$_{Hse155}$-ClAc (0.5 ns, 4 ns, 4.5 ns, 6 ns, 7 ns, and 9.5 ns).

Figure 2 Structures of reactant (R), transition state (TS), and product (P) involved in the defluorination process of system FAcD$_{Hse155}$-FAc at snapshot 4 ns. The unit for bond distances and imaginary frequency are in Å and cm^{-1}.

Figure 3 a, potential energy barriers versus angle O$_\varepsilon$C$_\delta$X variations (X means F for FAcD$_{Hse155}$-FAc and Cl for FAcD$_{Hse155}$-ClAc), b, potential energy barriers versus values of angle O$_\varepsilon$C$_\delta$X in reactants, c, potential energy barriers versus values of angle O$_\varepsilon$C$_\delta$X in transition states.

Figure 4 $\Delta E^{\text{i-0}}$ values of twenty individual residues toward defluorination and dechlorination processes of FAcD.

519
520
521
522
523
524
525
526

FAcD$_{Hsd155}$-FAc (Reactant)   **FAcD$_{Hse155}$-FAc (Reactant)**   **FAcD$_{Hse155}$-ClAc (Reactant)**
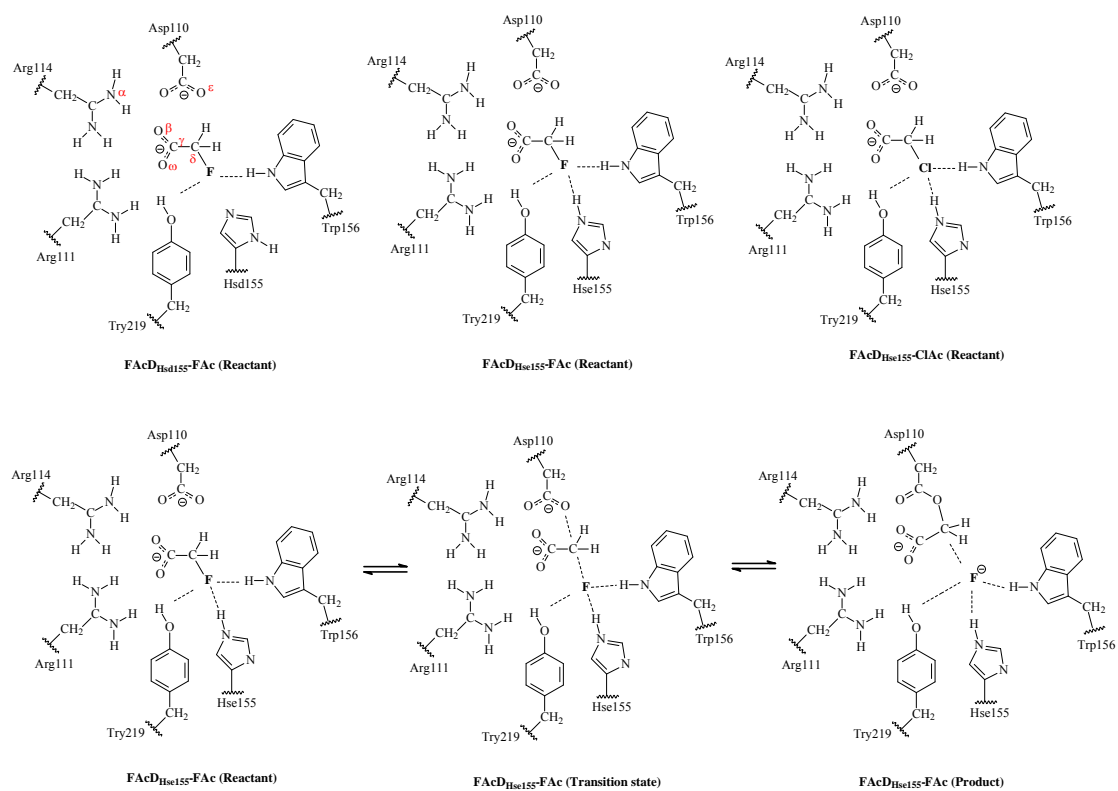
527   **FAcD$_{Hse155}$-FAc (Reactant)**   **FAcD$_{Hse155}$-FAc (Transition state)**   **FAcD$_{Hse155}$-FAc (Product)**
528
529
530
531
532
533
534
535
536
537
538
539   **Scheme 1**
540
541
542
543
544

24

545
546
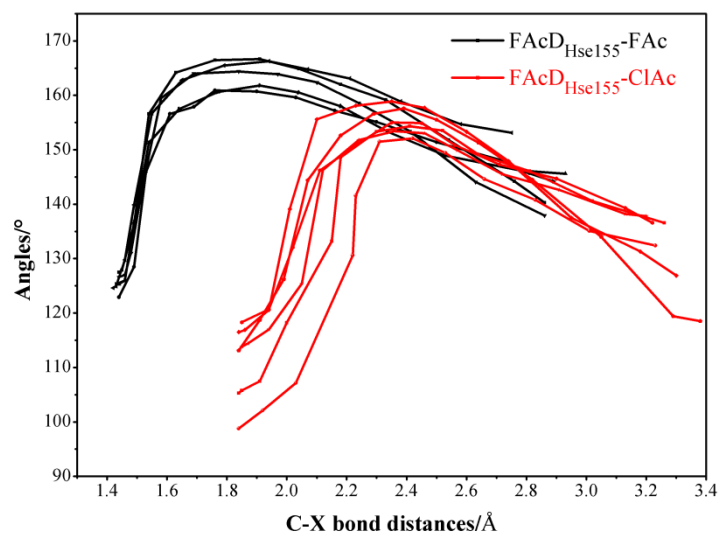
547
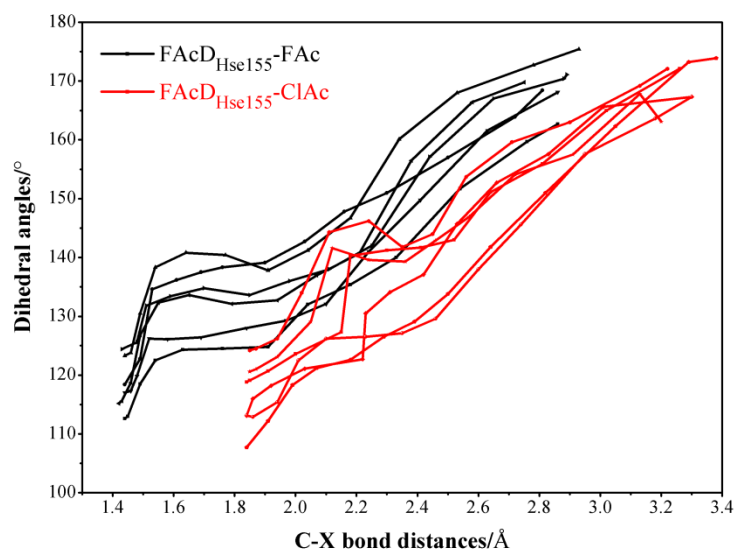
548
549
550
551
552
553
554
555
556
557 **Figure 1**
558
559
560
561
562

563
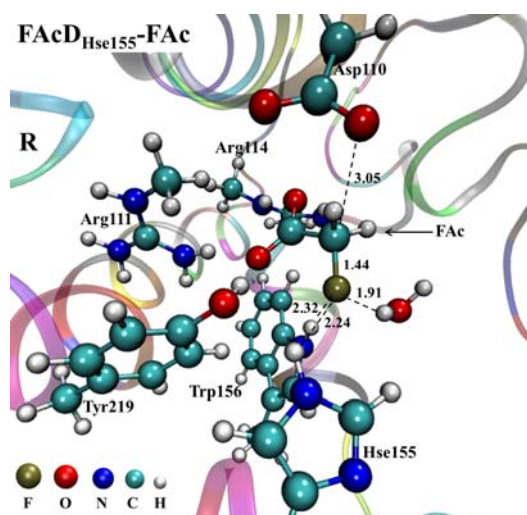
564
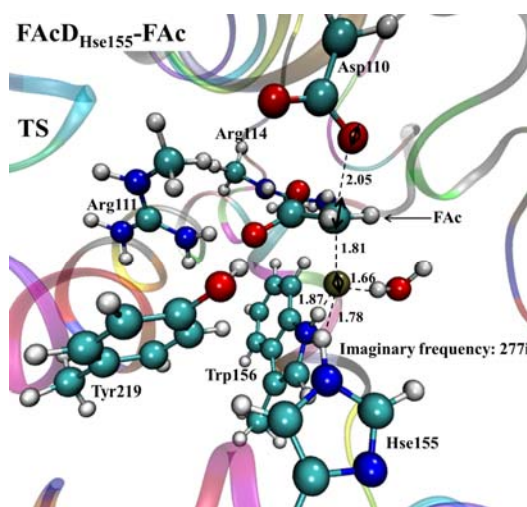
565
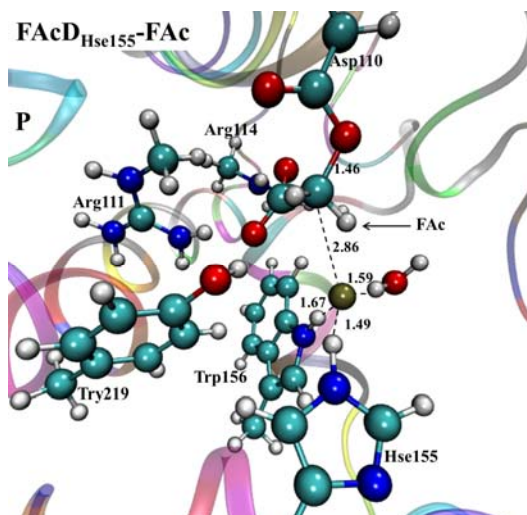
566

567 **Figure 2**

568

569

570
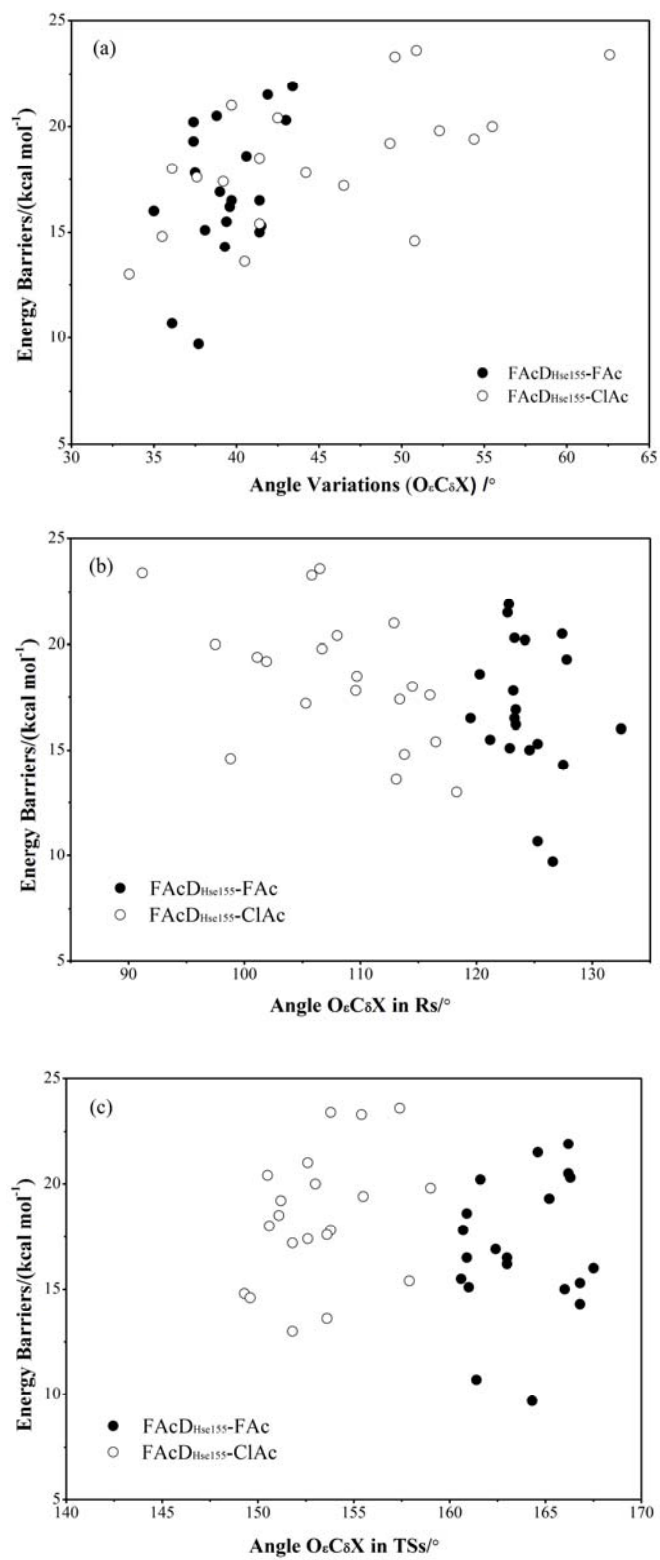
571

572

573

574

575

576

577   **Figure 3**

578

579

580

581
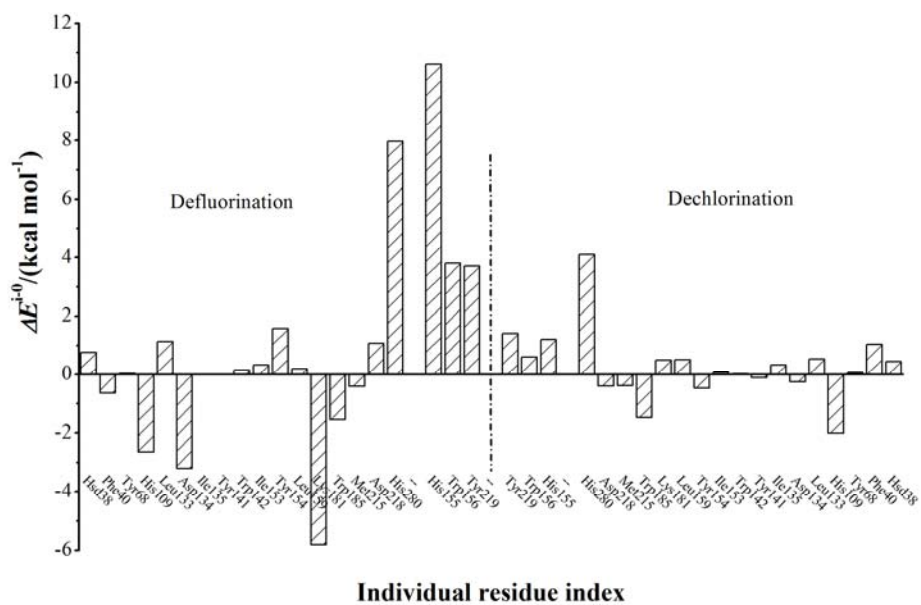
582

583

584

585

586

587

588

589

590   **Figure 4**

591

592

593

Key Structural Parameters   *vs.*   **Potential Energy Profiles**

Graphical Abstract
102x50mm (300 x 300 DPI)